ELSEVIER

Journal of Nuclear Materials 264 (1999) 10–19

journal of nuclear materials

Densification behaviour of UO_2–50%PuO_2 pellets by dilatometry

T.R.G. Kutty *, P.V. Hegde, R. Keswani, K.B. Khan, S. Majumdar, D.S.C. Purushotham

Radiometallurgy Division, Bhabha Atomic Research Centre, Trombay, Mumbai 400 085, India

Received 22 January 1998; accepted 10 August 1998

Abstract

The sintering behaviour of UO_2–50%PuO_2 pellets has been studied using a dilatometer in inert, reducing and oxidising atmospheres. The shrinkage begins at a much lower temperature in oxidising atmosphere such as CO_2 and commercial N_2. The shrinkage rate was found to be maximum for pellets sintered in N_2 atmosphere. The mechanism for the initial stage of sintering was found to be volume diffusion for both oxidising and reducing atmospheres. The activation energy for the initial stages of sintering was found to be 365 and 133 kJ/mol for Ar–8%H_2 and CO_2 atmospheres, respectively. The activation energy obtained using the Dorn method matches well with that obtained using the rate controlled sintering process. The lower activation energy obtained in the oxidising atmosphere is explained with the help of models available in the literature.

PACS: 81.20.Ev; 61.72.-y; 66.30.Fq

1. Introduction

The mixed uranium plutonium carbide, $(U_{0.3}Pu_{0.7})C$, is used as the driver fuel in the Indian Fast Breeder Test Reactor (FBTR) at Kalpakkam. So far this fuel has seen a burn up of around 35,000 MWD/T. The fuel for the second core of FBTR has been tentatively fixed as $(U_{0.45}Pu_{0.55})C$. The carbide fuel has many advantages over oxide fuel in such points as better thermal conductivity and higher metal atom density which in turn leads to higher linear power rating and superior breeding ratio [1–3]. However, there are some disadvantages associated with the nature of carbide. Carbide is not only pyrophoric and susceptible to oxidation in an atmosphere containing oxygen but it easily hydrolyses by moisture. Therefore, the entire fuel fabrication has to be carried out in inert atmosphere that makes the fuel fabrication very costly. The difficulty of dissolution of carbide in HNO_3 poses a problem with regard to the reprocessing of the spent fuel.

A possible alternative fuel to $(U_{0.45}Pu_{0.55})C$ for FBTR is the oxide fuel of composition UO_2–50%PuO_2. However, very little information is available in the literature on its properties and behaviour. The present study deals with the sintering behaviour of the above mentioned mixed oxide using a dilatometer in various atmospheres of Ar, Ar–8%H_2, CO_2 and commercial N_2 gases. The kinetics of sintering and the mechanism of sintering have also been studied.

UO_2 and PuO_2 are of fluorite structure and have very high melting points. The single phase field of UO_2 is very wide extending from the O/U ratio of 1.65 to 2.25 [4]. The substoichiometric oxide exists only at very high temperature whereas hyperstoichiometric oxide exists even at very low temperature. The PuO_2 phase field is stable within the O/Pu ratio of 1.61 to 2.0 [5]. The stoichiometric PuO_2 can be made substoichiometric by heating in reducing/inert atmosphere. The hyperstoiochiometric PuO_2 is not known and presumably does not exist. UO_2 can dissolve large amounts of oxygen to the interstitial

* Corresponding author. Tel.: +91-22 556 6950; fax: +91-22 556 0750; e-mail: rmd@magnum.barc.ernet.in.

0022-3115/99/$ – see front matter
PII: S0022-3115(98)00490-5

sites forming anion excess UO_{2+x}, and PuO_2 or (U, Pu)O_2 can accommodate large concentration of oxygen vacancies in the reduced state forming anion deficient PuO_{2-x} or (U, Pu)O_{2-x}. Thus the dominant defects in UO_2, PuO_2 and (U, Pu)O_2 are anion Frenkel defects, O^{2-} vacancies and O^{2-} interstitials [6,7].

Enough work has been reported on the shrinkage behaviour UO_2 and ThO_2 but not much has been reported on (U, Pu)O_2 having high PuO_2 content. The interdiffusion coefficient in UO_2–PuO_2 system is strongly dependent on Pu content, temperature and oxygen potential [6]. It is well known that the diffusion coefficient of U and Pu in $UO_{2\pm x}$ and $MO_{2\pm x}$ (M = U, Pu) varies by 4–5 orders of magnitude at constant temperature, if oxygen potential is varied [7,8]. Diffusion rate is low under reducing condition and is fast under oxidising condition. Since diffusion is largely dependent on oxygen potential of the sintering atmosphere, it will be worthwhile to determine the effects of such various types as inert(Ar), reducing (Ar–8H_2) and oxidising (CO_2 and commercial N_2) atmospheres on its sintering behaviour. In this work, the mechanisms of sintering during the initial stage of sintering have been determined using rate controlled sintering technique. The activation energy for the process was evaluated by the Dorn method [9,10].

2. Theory

2.1. Rate controlled sintering

The rate controlled sintering (RCS) was first proposed by Palmour et al. [11–13] to describe the sintering where the densification rate is controlled rather by heating rate. The measurement of this process, using a dilatometer, is very useful for studying the sintering mechanism of powder compacts during the initial stages of sintering. RCS results in formation of fine grain size pellet, avoids gas entrapment in pores and minimises pore-grain boundary separation [14,15]. The principle of RCS is as follows.

The green compact is heated in a dilatometer at a constant heating rate until d*l*/d*t*, i.e. slope of the length vs. time curve, becomes larger than a threshold value, at which point the temperature rise is stopped. The shrinkage now takes place under isothermal condition. On completion of sintering at this temperature, which is shown by the smaller d*l*/d*t* signal than a second threshold value, the temperature rise is resumed and the process is repeated as shown in Fig. 1.

The experimental shrinkage curve obtained by dilatometry generally follows an equation of the form [14],

$$\Delta l/l_0 = Y = [K(T)t]^n, \tag{1}$$

where l_0 is the initial length of the sample at the start of the sintering, $K(T)$ the Arrhenius constant, t the time

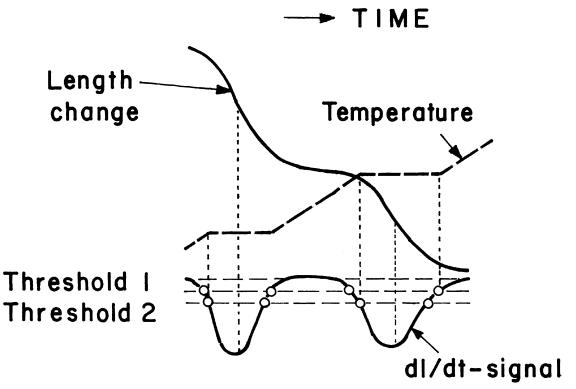

Fig. 1. A schematic drawing of rate controlled sintering process. The change in length and shrinkage rate (d*l*/d*t*) occurring in each isothermal step is shown. The upper and lower threshold values are shown as threshold 1 and threshold 2, respectively.

and n a constant whose value depends on the sintering mechanism.

Many models of sintering have been presented and discussed in the literature [16–20]. A sintering model proposed by Johnson [21], in which all the significant mechanisms of materials transport can be identified even though more than one mechanism may be operating simultaneously, has been used in this study. If it is assumed that all the material in the neck comes from grain boundary and if the material transport by surface diffusion, vapour transport are insignificant, then the shrinkage for the first 3.5% can be expressed as [21]

$$Y^{2.06}\dot{Y} = (2.63\gamma\Omega D_v/kTa^3)Y^{1.03} + (0.7\gamma\Omega bD_b/kTa^4), \tag{2}$$

where γ is the surface tension, Ω the vacancy volume, D the diffusion coefficient, T the temperature, a the particle radius, b the thickness of the grain boundary and k the Boltzmann constant.

If only the volume diffusion from grain boundary is operative, then Eq. (2) becomes [21]

$$Y = (5.34\gamma\Omega D_v/kTa^3)^{0.49}t^{0.49}. \tag{3}$$

Similarly for grain boundary diffusion

$$Y = (2.14\gamma\Omega bD_b/kTa^4)^{0.33}t^{0.33}. \tag{4}$$

Eqs. (3) and (4) predict the slopes of 0.49 and 0.33 in a plot of ln Y vs. ln t for volume diffusion and grain boundary diffusion, respectively.

On differentiating Eqs. (3) and (4) with respect to time, we get

$$\dot{Y} = 0.49(5.34\gamma\Omega D_v/kTa^3)^{0.49}t^{-0.51}, \tag{5}$$

$$\dot{Y} = 0.33(2.14\gamma\Omega bD_b/kTa^4)^{0.33}t^{-0.67}. \tag{6}$$

The slope of the plot of ln $\dot{Y}$ vs. ln t will be $(n-1)$ from which the sintering exponent 'n' can be evaluated. From the value of Y intercepts, the diffusion coefficient can be evaluated. The variation of log D with T can be described by an equation of the type

$$D = D_0 \exp(-Q/RT), \tag{7}$$

where D_0 is the pre-exponential factor and Q the activation energy.

2.2. Dorn method for the determination of activation energy

This method enables to determine the activation energy for the initial stages of sintering using a single sample. It thus eliminates parameters which may vary from sample to sample. The Dorn method involves the measurement of shrinkage rate immediately before and after an instantaneous temperature increase of the order of 30°C.

Originally, Dorn [22] used this method to determine the activation energy of creep. A sample was allowed to deform under a constant tensile stress at temperature T_1, and then the temperature was rapidly raised or lowered to a new value T_2 allowing the sample to deform further. If the strain rates at temperatures T_1 and T_2 are ϵ_1 and ϵ_2, respectively, then the activation energy Q is given by [22]

$$Q = RT_1T_2/(T_1 - T_2) \ln \epsilon_2/\epsilon_1. \tag{8}$$

Bacmann and Cizeron [9,10] applied the above mentioned method to determine the activation energy during the initial stages of sintering of UO_2 by using a relation similar to the above equation:

$$Q = RT_1T_2/(T_1 - T_2) \ln v_2/v_1, \tag{9}$$

where v_2/v_1 is the ratio of the shrinkage rates measured at the point of temperature change. The composition and structural state of the sample should remain constant during the temperature change for the validity of this method. If the rate of temperature increase is rapid and temperature difference ΔT is small, then the composition and structural state of the sample can be assumed to remain constant at the point when rapid temperature change is effected.

3. Experimental

3.1. Fabrication of green pellet

The green pellets for this study, were prepared by the conventional powder metallurgy technique involving mixing and cold compaction. The UO_2 and PuO_2 powders were milled for 4 h in a planetary ball mill using tungsten carbide balls. The blended powder was precompacted, granulated and finally compacted at around 300 MPa to green pellets of 4.6 mm diameter and around 8 mm in length. The density of green pellets was 52 ± 1% of theoretical density (TD).

To facilitate compaction and to impart handling strength to the green pellets, 1 wt% zinc behenate was added as lubricant/binder during the last hour of milling. The characteristics of UO_2 and PuO_2 powders used in this study are given in Table 1.

3.2. Dilatometry

The shrinkage behaviour of the UO_2–50%PuO_2 compacts in the various atmospheres was studied using a push rod type dilatometer. The shrinkage was measured in axial direction. The sample supporter, measuring unit and displacable furnace of the dilatometer were mounted horizontally. The measurements were made by an LVDT transducer which was maintained at a constant temperature by means of water circulation from a constant temperature bath. The temperature was measured using a thermocouple which is placed directly above the sample. A small force of 0.2 N was applied on the sample through the push rod. The dilatometric experiments were carried out using a flow rate of 18 l/h and a heating rate of 6°C/min. The impurity contents of the cover gases used in this study are given in Table 2.

The selection of the temperature programme was controlled by a computer via data acquisition system. Correction was applied for the expansion of the system by taking a run under identical condition using a standard sample (POCO graphite, NIST).

3.3. Shrinkage kinetics

For RCS, the temperature programme was modified in such a way that the whole sintering took place between two shrinkage rates as described in Section 2.1. The heating rate used for RCS was 6°C/min and gas flow rate was 18 l/h.

Table 1
Characteristics of UO_2 and PuO_2 powders

Property	UO_2	PuO_2
Oxygen to metal ratio	2.10	2.00
Apparent density (g/cm^3)	1.5	1.2
Total impurities (ppm)	<800	<1200
Theoretical density, ρ (g/cm^3)	10.96	11.46
Surface energy, γ (erg/cm^2) [55]	600	570 [b]
Particle radius [a], a (Å)	489	97
Specific surface area, S (m^2/g)	2.8	13.6

[a] $a = 6/(2\rho Sf)$ where f is the shape factor.
[b] γ_{PuO_2} value is obtained from the relation: $\gamma_{PuO_2}/\gamma_{UO_2} = 0.95$ [55].

Table 2
Impurity contents of different sintering atmospheres

Sintering atmosphere	Oxygen (ppm)	Moisture (ppm)	CO_2 (ppm)	CO (ppm)	N_2 (ppm)	Oxides of N_2 (ppm)	Hydrocarbon (ppm)
Argon	4	4	1	1	10	1	1.5
Argon +8% hydrogen	4	4	1	1	10	1	2
Carbon dioxide	300–400	10	–	5	50	15	2
Commercial nitrogen	400–500	10	50	5	–	–	5

For the Dorn method, the sample was heated at a rate of 6°C/min to a temperature (1160°C and 732°C for Ar–8%H_2 and CO_2 atmospheres, respectively) at which the shrinkage just began. The shrinkage was then allowed to continue isothermally for about an hour at this temperature. The temperature of the sample was then quickly raised by ~30°C at a rate of 20°C/min and held at this temperature. This process was repeated until a total shrinkage attained around ~3%.

The sintering kinetics of UO_2–50%PuO_2 pellets have been evaluated only in Ar–8%H_2 and CO_2 atmospheres, which are the most commonly used atmospheres for sintering the mixed oxides.

3.4. Characterization

The UO_2–50%PuO_2 pellets sintered in different atmospheres were characterised in terms of their density, oxygen to metal ratio (O/M) and phase content. The O/M ratio was measured thermogravimetrically and the phase content was estimated by X-ray diffractometry and metallography. The X-ray diffraction patterns of the pellets were obtained by using the CuK_α radiation and graphite monochromator. For metallography, the sintered pellet was mounted in bakelite and ground using successive grades of emery paper. The final polishing was done using diamond paste. The etching has been carried out using a mixture of 30% HNO_3 containing a few drops of ammonium biflouride at 60°C.

4. Results

Fig. 2 shows the shrinkage curve (dl/l_0) for UO_2–50%PuO_2 pellet in Ar–8%H_2 atmosphere. The shrinkage rate as a function of temperature is also shown in the same figure. Fig. 3 compares the shrinkage behaviour of the same composition sample in Ar, Ar–8%H_2, CO_2 and commercial N_2. Fig. 4 compares the shrinkage rate as a function of temperature in the above mentioned atmospheres.

To verify the accuracy of the measurements, a few runs were repeated. Fig. 5 shows the shrinkage curve obtained during two runs for UO_2–50%PuO_2 pellet. The second run was found to give the same results as the first run.

From Fig. 3, it can be seen that the shrinkage curves for UO_2–50%PuO_2 in Ar and Ar–8%H_2 are almost identical up to 1000°C. Above 1100°C the shrinkage is faster in Ar–8%H_2 than in pure Ar. The maximum shrinkage observed at 1650°C for Ar and Ar–8%H_2 was 16% and 17%, respectively.

In CO_2, the shrinkage starts at a much lower temperature. The pellet started to shrink at around 600°C in

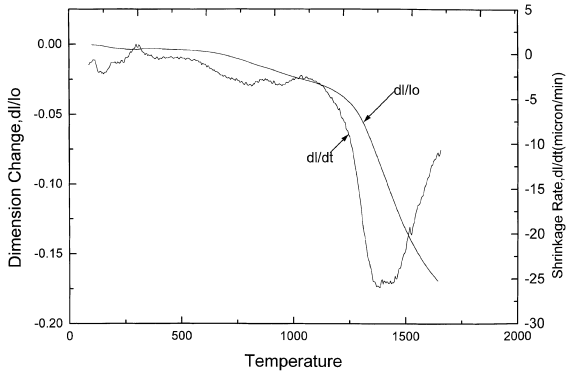

Fig. 2. Shrinkage curve for UO_2–50% PuO_2 pellet in Ar–8%H_2 atmosphere. The dl/l_0 values are plotted against temperature, where l_0 is the initial length of the pellet.

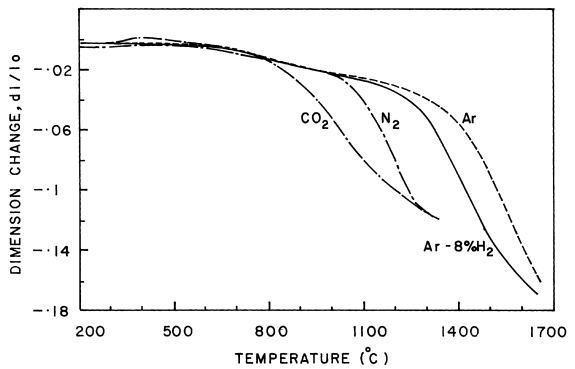

Fig. 3. Comparison of the shrinkage behaviour of UO_2–50% PuO_2 pellet in Ar, Ar–8%H_2 , CO_2 and commercial N_2 atmospheres.

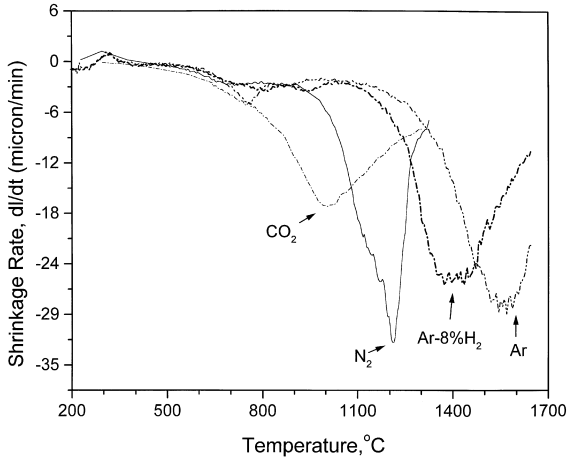

Fig. 4. Shrinkage rate (dl/dt) of UO_2–50% PuO_2 pellet in Ar, Ar–8%H_2, CO_2 and commercial N_2 atmospheres plotted against temperature.

CO_2 compared to 1100°C in Ar–8%H_2 atmosphere. A maximum shrinkage of ~12% was observed at 1350°C. A remarkable feature of dl/l_0 vs. T plot is the slight expansion observed at around 350°C. The shrinkage behaviour in N_2 is similar to the one observed in CO_2 showing a maximum shrinkage of ~12% at 1350°C. However the shrinkage begins at somewhat higher temperature (950°C) compared to that observed in CO_2. The notable feature in the shrinkage behaviour in N_2 atmosphere is a drastic shrinkage observed in the temperature range of 1000–1200°C.

The dl/dt vs. temperature plot for UO_2–50%PuO_2 green pellets shown in Fig. 4 indicates that a maximum shrinkage rate of 32 μm/min was obtained for pellets sintered in N_2 at 1200°C. For the pellets sintered in the other atmospheres, the maximum shrinkage rate was found to be 29, 26 and 15 μm/min, respectively, for the

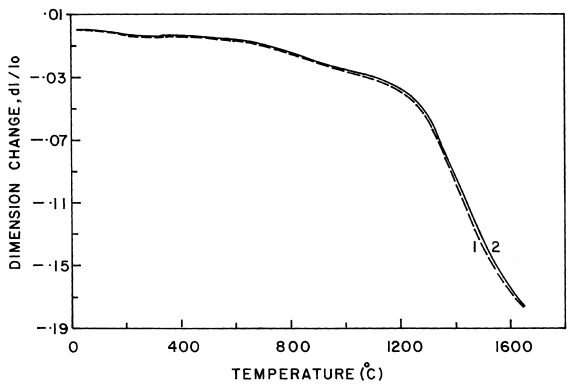

Fig. 5. Repeat runs showing reproducibility for UO_2–50% PuO_2 pellet in Ar–8%H_2. The numbers 1 and 2 represent the shrinkage curve for the first and second run.

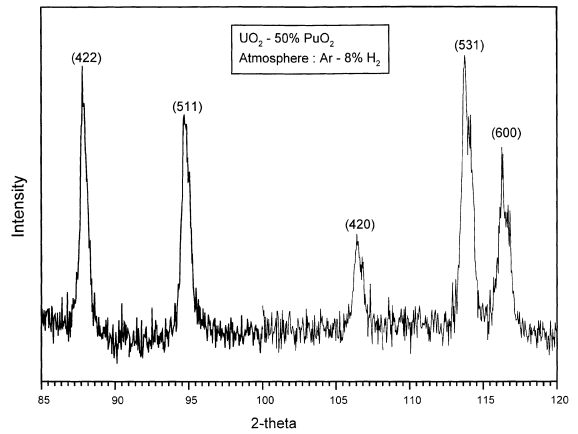

Fig. 6. XRD pattern of sintered UO_2–50% PuO_2 pellet sintered in Ar–8%H_2 atmosphere.

pellets sintered in Ar, Ar–8%H_2 and CO_2. This maximum was observed at 1550°C and 1400°C for Ar and Ar–8%H_2, respectively, while it was seen at a much lower temperature (~1000°C) for CO_2.

The XRD pattern of UO_2–50%PuO_2 pellets sintered in these atmospheres for 4 h showed only one phase. A typical XRD pattern of sintered UO_2–50%PuO_2 pellet is shown in Fig. 6. The precise lattice parameter was calculated using the least square method from the high angle lines and was found to be 5.440 Å. The geometrical density of UO_2–50%PuO_2 pellets sintered in Ar and Ar–8%H_2 was almost identical (89% TD) and that of pellets sintered in CO_2 and commercial N_2 was around 87% TD. The O/M values of pellets measured after sintering are given in Table 3. The typical impurity contents in a sintered pellet is shown in Table 4.

The microstructure of the sintered UO_2–50%PuO_2 pellet revealed a single phase structure. The microstructure of the pellet sintered in Ar–8%H_2 showed a distinct difference from that of the pellets sintered in other atmospheres (see Fig. 7). The as-polished structure of the above mentioned pellet showed the clusters of fine pores at many locations. The grains were duplex in nature with regions of very fine grains (<1 μm) surrounding big particles. These fine grained region formed a chain of interconnecting network.

Table 3
O/M ratio of UO_2–50%PuO_2 pellet after sintering

Sintering atmosphere	O/M ratio
Ar	1.97
Ar–8%H_2	1.87
CO_2	2.02
Commercial N_2	2.002

Table 4
Metallic impurities in UO_2–50%PuO_2 pellet

Element	Impurity (ppm)
Na	<50
Ca	<100
Al	<10
Mg	<25
Si	<90
Fe	<200
Cr	<80
Co	<5
Ni	<50
Mo	<10
W	<40
B	<0.18
Cu	<10
Zn	<10

5. Discussion

From the above results, it is clear that the shrinkage occurs more rapidly in oxidising atmosphere. A shrinkage of ~12% was obtained at 1300°C in CO_2 while it was only 6% in Ar–8%H_2 and 4% in Ar at the same temperature (see Fig. 3).

Chikalla [23,24] studied the sintering behaviour of UO_2–PuO_2 of various compositions in various atmospheres. He has observed that the addition of up to 10% PuO_2 reduced the sinterability of UO_2 in H_2. A complete solid solution formation has been reported on sintering both mixed and coprecipitated oxides in H_2 over a range of 0–100% PuO_2. Russel et al. [25] have investigated the rate at which the solid solution was formed between the two constituent oxides and found that the rate was quite slow in Ar at temperatures up to 1600°C and the rate was even slower in H_2 with a part of the PuO_2 remained in the reduced form of $PuO_{1.62}$. Brett and Russel [26] made a detailed investigation on UO_2 containing various amounts of PuO_2 in Ar, H_2 and CO_2. They reported a complete solid solution formation in Ar and CO_2 but reported two phased structure for pellets having high PuO_2 content (>40% PuO_2) sintered in H_2. Akutsu et al. [27] have also reported a single phase for pellets of UO_2–40%PuO_2 sintered in N_2–5%H_2 mixture. A continuous series of solid solution between PuO_2 and UO_2 has been reported by Mulford and Ellinger [28]. Russel et al. [29] have fabricated UO_2–50%PuO_2 pellets and studied its sintering behaviour. They reported a single phase for the pellets sintered in Ar and in H_2 at 1650°C.

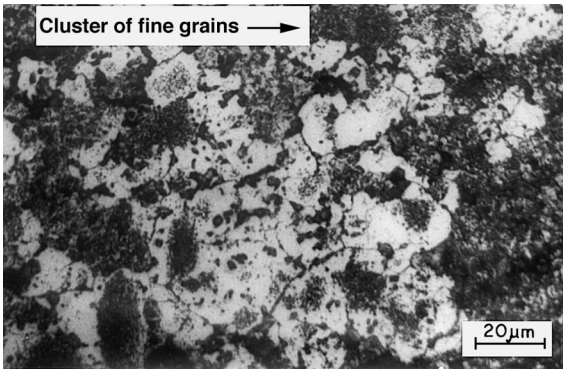

Fig. 7. Microstructure of UO_2–50% PuO_2 pellet sintered in Ar–8%H_2. The duplex grain structure can be noticed in this figure. The clusters of fine grains with size (<1 μm) form an interconnecting network.

The homogenisation and sintering of UO_2–PuO_2 compacts is a consequence of cation interdiffusion between UO_2 and PuO_2. It is postulated that the cation flux from UO_2 to PuO_2 grains is much larger than that from PuO_2 to UO_2 grains thus resulting a net transport of metal atom from UO_2 to PuO_2. The PuO_2 grains grow at the cost of UO_2 grains, pushing UO_2 grain boundaries inwards [30–32]. Theissen and Vollath [33] observed that PuO_2 particles surround a UO_2 particle with intermediate small interdiffusion zone. They noted that prior to appreciable homogenisation of the mixed compact, PuO_2 envelops UO_2 grains. Since bonding or neck growth between particles involves the gross migration of material, for MO_2 both M ions and oxygen transfer must occur. Since the oxygen diffusion rate is higher than that of M ions by 10^6, any bonding via volume diffusion must be kinetically limited by the U, Pu ion mobility [34].

Metal vacancies and interstitials are minority defects in UO_2 and MO_2 system. Because of their low mobility, the diffusion of U and Pu is the rate determining step for many high temperature processes such as sintering, creep, grain growth, homogenisation, solid solution formation etc. It is reported that D^U increases dramatically with x in UO_{2+x} at constant temperature by about a factor of 10^5 between $UO_{2.0}$ and $UO_{2.2}$ at 1700°C [7]. D^U and D^{Pu} in $(U, Pu)O_{2\pm x}$ depend strongly on oxygen partial pressure or O/M ratio with a minimum in diffusion rates at O/M = 1.98 at 1500°C. An approximate x^2 dependence in hyperstoichiometric region has also been reported for sintering, grain growth and creep [7,35].

Matzke [36–39] has made extensive studies on diffusion in the UO_2–PuO_2 system. He has measured interdiffusion in the system of UO_2/PuO_2 between 1400°C and 1800°C in a wide range of oxygen potential and for full range of Pu contents from 0 to 100%. The interdiffusion coefficients are a strong function of T, $\Delta\bar{G}(O_2)$ and Pu content. At constant Pu content, D^{Pu} increases by up to the two orders of magnitude if the equilibrium oxygen pressure changes from reducing to oxidising atmospheres. He has reported a vacancy mechanism for $MO_{2\pm x}$ for O/M > 1.98 and interstitial mechanism for

O/M < 1.98 [36]. However, the existence of high concentration of metal interstitials is unrealistic for low O/M values. A cluster mechanism is reported to dominate for O/M values below 1.95 [7].

Our experimental results show that the O/M ratios of UO_2–50%PuO_2 pellets sintered in Ar–8%H_2 and Ar are 1.87 and 1.97, respectively. For an O/M ratio of 1.97 obtained for Ar atmosphere, the interstitial mechanism is suggested. Since the H_2O/H_2 ratio of Ar–8%H_2 sintering gas used in this study was less than 10^{-4}, a highly reducing environment is ensured inside the sintering furnace. At such a reducing atmosphere, the charge state of most of Pu will be Pu^{+3}. The Pu^{+3} ions were shown to diffuse faster than Pu^{+4} ions in ThO_2–PuO_2 system [7]. Also U^{+5} ion was found to diffuse more slowly than U^{+4} ion in UO_{2+x}. The migration energies for U^{+4} and Pu^{+4} are identical (~6 eV) but the migration energy for U^{+5} is ~22% higher and that for Pu^{+3} is about 31% lower than that of U^{+4} and Pu^{+4}. The increased diffusion of Pu in (U, Pu)O_{2-x} at O/M < 1.98, is partly due to faster mobility of Pu^{+3} ions. Schmitz and Marajofsky [40] have given an alternative explanation for the observed increase in matter transport in MO_{2-x}. Since O/M is below 1.90 (see Table 3) for the pellets sintered in Ar–8%H_2, the major defects will be clusters. They have pointed out that two Pu^{+3} atoms connected to an oxygen vacancy (Pu^{3+}–V_o–Pu^{3+}, where V_o is the oxygen vacancy) would provide enhanced metal mobility via a type of ring mechanism [7].

In CO_2 and commercial N_2 atmospheres, the final O/M ratio of the pellets is >2.0 (see Table 3). The CO/CO_2 ratio of the sintering gas has been kept less than 10^{-4} ensuring a highly oxidising atmosphere. In this case, the Lidiard model [41] predicts a large increase in metal vacancy concentration and thus a high metal atom diffusion rate. This model is found to be applicable to oxidative sintering process in CO_2 or commercial N_2. Thus sintering under oxidising condition connected with fast diffusion can be achieved in short time.

The data obtained in this study clearly indicate that UO_2–50%PuO_2 pellets can be fabricated in oxidising atmosphere such as CO_2 or commercial N_2 at ~1300°C. The fabrication in Ar–8%H_2 atmosphere otherwise requires temperatures higher than 1650°C. The impurities in commercial N_2 (~500 ppm of O_2) help in achieving faster shrinkage at around 1200°C. N_2 has smaller ionic radius and better thermal conductivity than CO_2. This may also help for the rapid shrinkage of UO_2–50%PuO_2 pellets in N_2 at around 1100°C. Better shrinkage obtained in Ar–8%H_2 than Ar (see Fig. 3) is due to a large deviation of stoichiometry for pellets sintered in Ar–8%H_2 which enhances the sintering.

Another important point noticed during the densification is the retardation of densification at around 800°C in Ar and Ar–8%H_2 (see Figs. 3 and 4). The retardation of densification correlates with the onset of the solid solution formation. The solid solution is formed by the interdiffusion of Pu^{+4} ion into UO_2 lattice and U^{+4} ion into PuO_2 lattice. These interdiffusion processes decrease the sintering rate and shift densification to a higher temperature. Such phenomenon has been reported for UO_2–30%PuO_2 and UO_2–Gd_2O_3 fuels [42,43]. Matzke [36,37] has also reported about the formation of a diffusion barrier in his study on the diffusion couple between UO_2 and PuO_2 pellets. This has been attributed to the local variation of O/M ratio along the diffusion couple.

From the above discussion, it may be concluded that sintering under oxidising condition can be carried out at a temperature ~1300°C, which is about 300°C lower than that in reducing condition.

6. Kinetics of sintering

6.1. Rate controlled sintering

The sintering kinetics have been evaluated for reducing (Ar–8%H_2) and oxidising (CO_2) atmospheres for the initial stages of sintering. The kinetics have been evaluated in a small temperature range of ~80°C between 1160°C and 1247°C for Ar–8%H_2 and 732–812°C for CO_2 atmospheres. The H_2O/H_2 and CO/CO_2 ratios of the sintering gas (Ar–8%H_2 and CO_2) used in this study was kept smaller than 10^{-4} during this study.

Fig. 8 shows a typical plot showing the variation of dl/l_0 and dl/dt observed in each isothermal step. The parameter 'n' of Eq. (1) is obtained from the slope of log $\dot{Y}$ vs. log t plot which is shown in Fig. 9 for Ar–8%H_2 atmosphere. A similar plot for CO_2 is shown in Fig. 10. The value of n obtained for pellets sintered in Ar–H_2 at 1191°C, 1225°C and 1247°C is ~0.50. It was noted that the value of n was around 0.7–0.8 during the first few

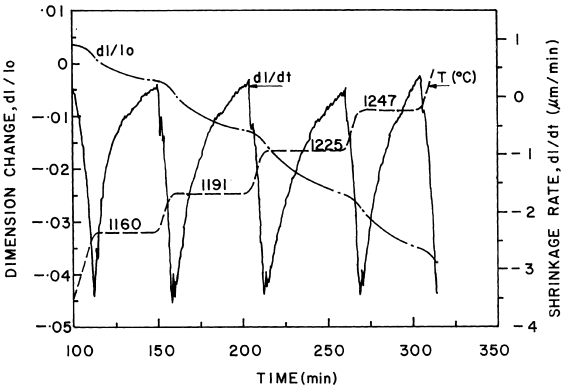

Fig. 8. Rate controlled sintering showing the variation in dl/l_0 and dl/dt occurring in each isothermal step. The atmosphere used was Ar–8%H_2.

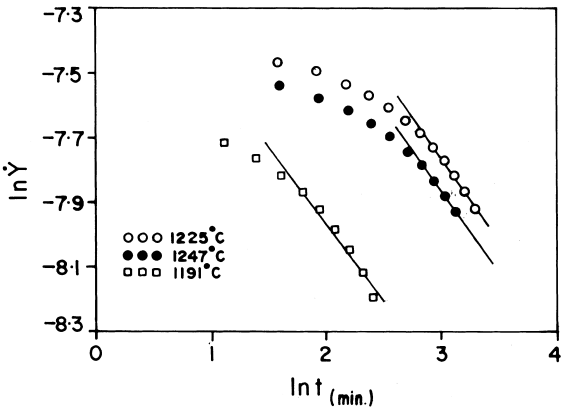

Fig. 9. A plot of ln $\dot{Y}$ vs. ln t for the pellet sintered in Ar–8%H_2. The slope of this curve will be $(n-1)$ from which the sintering exponent 'n' can be evaluated.

minutes of shrinkage. A similar phenomenon has been reported by Astier et al. [44] for their studies on rutile. This may be due to the fact that the sample may not be reaching a thermal equilibrium immediately after attaining the measuring temperature. Hence first several points of the data were discarded and not used in this study.

The value of n obtained at 758°C, 782°C and 812°C in CO_2 atmosphere is ~0.51. This value suggests that the mechanism of sintering in Ar–8%H_2 and CO_2 is the same since the value of n is almost the same. The values of n at 732°C in CO_2 and at 1160°C in Ar–8%H_2 were found to be higher than 1, and do not fit to any model available in the literature and therefore not used in this study. Since the value of n is around 0.50, the mechanism for shrinkage during the initial stage of sintering in CO_2 is volume diffusion. This is contrary to an earlier observation by Aybers for UO_2, (U, Th)O_2, (U, Pu)O_2 [45,46] where he found that the mechanism changes with atmosphere used for sintering. He has proposed that the mechanisms during initial stage of sintering are volume and grain boundary diffusion in reducing and oxidising atmospheres, respectively. El-Sayed Ali and Sorensen [47,48] have found $n=0.32$ in CO_2 atmosphere for (U, Pu)O_2 and $n=0.45$ in reducing atmosphere.

The diffusion coefficients are calculated from the intercepts in Figs. 9 and 10 using Eqs. (5) and (6). The values of parameters used for this calculation are given in Table 1. The ln D vs. $1/T$ plots for Ar–8%H_2 and CO_2 atmospheres are given in Figs. 11 and 12, respectively. The activation energies obtained for UO_2–50%PuO_2 in Ar–8%H_2 and CO_2 are 365 and 133 kJ/mol, respectively. The activation energies obtained by the Dorn method were found to be 376 and 138 kJ/mol for Ar–8%H_2 and CO_2 atmospheres, respectively, which are in close agreement with the value obtained using the RCS process.

A few pellets used for RCS studies were checked for their O/M ratio since they have not been fully sintered. The O/M value was found to be 1.94 for Ar–8%H_2 atmosphere. This clearly indicates that the pellet has considerably deviated from stoichiometry even at ~1250°C.

There is no report available in the literature about the activation energy for UO_2–50%PuO_2 composition. Hence no comparison is possible. The activation energy for U, Pu diffusion in (U, Pu)O_2 has been reported as

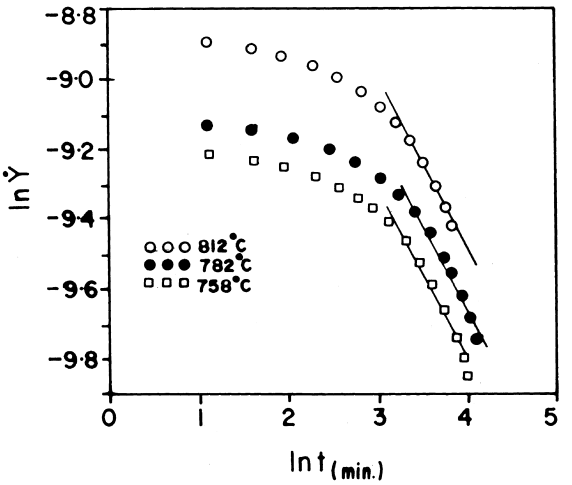

Fig. 10. A plot of ln $\dot{Y}$ vs. ln t for the pellet sintered in CO_2. The slope of this curve will be $(n-1)$ from which the sintering exponent 'n' can be evaluated.

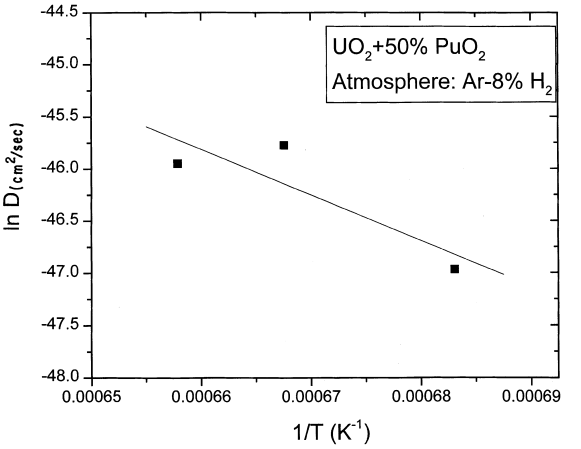

Fig. 11. The Arrhenius plot ln D vs. $1/T$ for UO_2–50% PuO_2 pellet sintered in Ar–8%H_2. The slope of this curve will be Q/R from which the activation energy Q can be estimated.

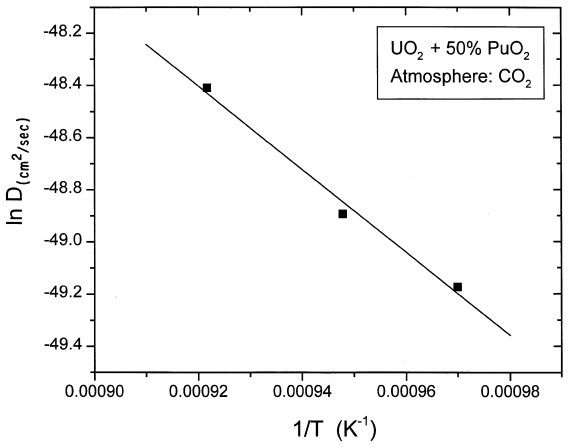

Fig. 12. The Arrhenius plot ln D vs. $1/T$ for UO_2–50% PuO_2 pellet sintered in CO_2.

~543 kJ/mol [37,52–54]. This value has been reported for stoichiometric material and is much higher than the value obtained in this study.

The point defect model [7,41] suggests that the difference in cation diffusion activation energies by vacancy process for hypostoichiometric and hyperstoichiometric oxide should be twice the anion Frenkel formation energy. The experimental evidence shows that this difference is ~5.2 eV which is much less than twice the best estimate for Frenkel formation enthalpy of 3.8 eV [49–51]. The difference in activation energies between reducing and oxidising atmospheres obtained in this study was found to be ~240 kJ/mol (~2.5 eV) which is much less than the theoretical value. Schmitz and Marajofsky [40] have given an interesting alternative to interstitial mechanism to explain the increase in D^{Pu} with decreasing O/M ratio. They proposed an interstitial ring mechanism which results in a change of place of U and Pu atoms. This mechanism suggests that two Pu atoms always remain in close proximity to an oxygen vacancy and the migration of U is in the opposite direction to that of the Pu. The low activation energy obtained in this study in Ar–8%H_2 could also be explained by the different kinds of defects and clusters present in the sample. It is reported that clusters of the type Pu^{3+}–V_o–Pu^{3+} is stable even at 1600°C [7].

For the pellets sintered in CO_2, the activation energy obtained is 133 kJ/mol which is much smaller than the activation energy for self-diffusion. The observed increase in D^{Pu} in MO_{2+x} is a strong argument in favour of vacancy mechanism [7]. The charge state of Pu under such condition will be largely Pu^{+4} and a part of U ions will be in a state of U^{+5}. The increase in the defects concentration has resulted in a lower activation energy for the pellets sintered in CO_2.

7. Conclusions

The sintering behaviour of UO_2–50%PuO_2 was studied in various atmospheres such as inert, reducing and oxidising atmospheres. The following conclusions were drawn:

1. Shrinkage begins at a much lower temperature in oxidising atmosphere such as CO_2 and commercial N_2.
2. The shrinkage behaviour is almost identical in Ar and Ar–8%H_2 up to 1100°C. Above this temperature, the shrinkage is rapid in Ar–8%H_2.
3. The densification process is retarded in temperature range from 800°C to 1000°C in Ar and Ar–8%H_2. This result was interpreted as due to the formation of solid solution.
4. The shrinkage rate was the highest for N_2 atmosphere.
5. The mechanism for the initial stage of sintering was found to be volume diffusion for both oxidising and reducing atmospheres.
6. The activation energy for sintering was found to be 365 and 133 kJ/mol for Ar–8%H_2 and CO_2 atmospheres, respectively.
7. The activation energy obtained using the Dorn method matches well with that obtained using the RCS process.
8. The lower activation energy in oxidising atmosphere is explained with the help of models available in the literature.

Acknowledgements

The authors had several useful discussions with Mr H.S. Kamath, Head, Advanced Fuel Fabrication Facility, Tarapur, whom they wish to acknowledge for his suggestions and comments. They are also grateful to Mr J.K. Ghosh, Dr A.K. Sengupta, Dr G.C. Jain, Messrs V.D. Pandey, T. Jarvis, K. Ravi, P. Sankaran Kutty, G.P. Mishra and T.S. Rao for their support during the course of this work.

References

[1] C. Ganguly, G.C. Jain, P.V. Hegde, U. Basak, R.S. Mehrotra, S. Majumdar, P.R. Roy, Nucl. Technol. 72 (1986) 59.
[2] Hj. Matzke, Science of Advanced LMFBR Fuels, North-Holland, Amsterdam, 1986, p. 1.
[3] C. Ganguly, P.V. Hegde, A.K. Sengupta, IAEA-TEC-DOC-466, IAEA, Vienna, 1988, p. 7.
[4] Hj. Matzke, Philos. Mag. 64A (1991) 1181.
[5] H.A. Wriedt, Bull. Alloy Phase Diagram 11 (1990) 184.
[6] C.R.A. Catlow, J. Chem. Soc. Faraday Trans. 83 (2) (1987) 1065.

[7] Hj. Matzke, in: T. Sorensen, Nonstoichiometric Oxides, Academic Press, New York, 1981, p. 156.
[8] J.R. Mathews, J. Chem. Soc. Faraday Trans. 83 (2) (1987) 1273.
[9] J.J. Bacmann, G. Cizeron, J. Am. Ceram. Soc. 51 (1968) 209.
[10] J.J. Bacmann, G. Cizeron, C.R. Acad. Sci. Paris Ser. C 264 (1969) 2077.
[11] H. Palmour III, M.L. Huckabee, T.M. Hare, in: M.M. Rustic (Ed.), Sintering – New Developments, Elsevier, Amsterdam, 1979, p. 46.
[12] M.L. Huckabee, H. Palmour, Ceram. Bull. 51 (1972) 574.
[13] H. Palmour, D.R. Johnson, in: G.C. Kuczynski, N.A. Hooton, C.F. Gibbs (Eds.), Sintering and Related Phenomena, Gordon and Breach, New York, 1967, p. 779.
[14] D.S. Perera, M.W.A. Stewart, Mater. Forum 20 (1996) 145.
[15] H. Kramer, J. Mater. Sci. Lett. 14 (1995) 778.
[16] D.L. Johnson, T.M. Clarke, Acta Metall. 12 (1964) 1173.
[17] R.L. Coble, J. Am. Ceram. Soc. 41 (1958) 55.
[18] D.L. Johnson, I.B. Cutler, J. Am. Ceram. Soc. 46 (1963) 541.
[19] W.D. Kingery, M. Berg, J. Appl. Phys. 26 (1955) 1205.
[20] L. Berrin, D.L. Johnson, in: G.C. Kuczynski, N.A. Hooton, C.F. Gibbs (Eds.), Sintering and Related Phenomena, Gordon and Breach, New York, 1967, p. 369.
[21] D.L. Johnson, J. Appl. Phys. 40 (1969) 192.
[22] J.E. Dorn, in: R. Maddin (Ed.), Creep and Recovery, Am. Soc. for Metals, Ohio, 1957, p. 255.
[23] T.D. Chikalla, Hanford Atomic Products Operation Report, Richland, Washington, HW-63081, 1959.
[24] T.D. Chikalla, Hanford Atomic Production Operation Report, Richland, Washington, HW-60276, 1959.
[25] L.E. Russell, N.H. Brett, J.D.L. Harrison, J. Williams, A.G. Adwick, Atomic Energy Research Establishment, Harwell Report AERE-R-3519, 1960.
[26] N.H. Brett, L.E. Russel, Atomic Energy Research Establishment, Harwell Report AERE-R 3900, 1962.
[27] H. Akutsu, K. Yoshioka, Y. Nakamura, Plutonium as a Reactor Fuel, IAEA, Vienna, 1967, p. 335.
[28] R.N.R. Mulford, F.H. Ellinger, J. Am. Chem. Soc. 80 (1958) 2023.
[29] L.E. Russel, N.H. Brett, J.D.L. Harrison, J. Williams, J. Nucl. Mater. 5 (1962) 216.
[30] R. Verma, P.R. Roy, Bull. Mater. Sci. 7 (1985) 21.
[31] S. Bataller, M. Ganivet, H. Guillet, Y. Masselot, F. Stosskopf, Plutonium as a Reactor Fuel, IAEA, Vienna, 1967, p. 301.
[32] H. Andriessen, R. Horne, J.M. Leblanc, M. Stievenart, W. Van Lierde, Plutonium as a Reactor Fuel, IAEA, Vienna, 1967, p. 237.
[33] R. Theisen, D. Vollath, Plutonium as a Reactor Fuel, IAEA, Vienna, 1967, p. 253.
[34] K.W. Lay, R.E. Carter, J. Nucl. Mater. 30 (1969) 74.
[35] G.E. Murch, C.A. Catlow, J. Chem. Soc. Faraday Trans. 83 (2) (1987) 1157.
[36] Hj. Matzke, J. Chem. Soc. Faraday Trans. 86 (1990) 1243.
[37] Hj. Matzke, J. Chem. Soc. Faraday Trans. 83 (2) (1987) 1121.
[38] Hj. Matzke, Atomic Energy Canada Ltd., Report AECL-2585, 1966.
[39] Hj. Matzke, J. Phys. 34 (1973) 317.
[40] F. Schmitz, A. Marajofsky, in: Thermodynamics of Nuclear Materials 1974, vol. 1, IAEA, Vienna, 1975, p. 467.
[41] A.B. Lidiard, J. Nucl. Mater. 19 (1966) 106.
[42] R. Manzel, W.D. Dorr, Bull. Am. Ceram. Soc. 59 (1980) 601.
[43] W. Dorr, S. Hellmann, G. Mages, J. Nucl. Mater. 140 (1986) 7.
[44] M. Astier, G. Brula, F. Lecomte, J.P. Reymond, P. Vergnom, in: M.M. Rustic (Ed.), Sintering – New Developments, Elsevier, New York, 1979, p. 150.
[45] M. Aybers, J. Nucl. Mater. 226 (1995) 27.
[46] M. Aybers, J. Nucl. Mater. 210 (1994) 73.
[47] M. El Sayed Ali, O.T. Sorensen, J. Thermal Anal. 25 (1982) 175.
[48] M. El Sayed Ali, O.T. Sorensen, in: B. Miller (Ed.), Proceedings of Seventh International Conference on Thermal Analysis, Wiley, New York, 1982, p. 344.
[49] R. Lindner, D. Reiman, F. Schmitz, Plutonium as a Reactor Fuel, IAEA, Vienna, 1967, p. 265.
[50] Hj. Matzke, in: H. Blank, R. Lindner (Eds.), Plutonium 1975 and Other Actinides, North-Holland, Amsterdam, 1976, p. 801.
[51] Hj. Matzke, Euratom Report EUR-770, 1982, p. 139.
[52] Hj. Matzke, R.A. Lambert, J. Nucl. Mater. 64 (1977) 211.
[53] D. Glasser-Leme, Hj. Matzke, Solid State Ionics 12 (1984) 217.
[54] D. Glasser-Leme, Hj. Matzke, J. Nucl. Mater. 106 (1982) 211.
[55] D.A. Mortimer, AERE Report AERE-7751, 1974.